SUPPORTING INFORMATION:

Dealloying Multiphase AgCu Thin Films in Supercritical CO_2

*Rachel Morrish and Anthony J. Muscat**

Department of Chemical and Environmental Engineering

University of Arizona, Tucson AZ 85721

High magnification images of AgCu films before and after dealloying

Figure S1 shows top-down and cross-sectional FESEM images of the AgCu films before and after dealloying. Note that in order to view the compositional contrast, the thin layer of CuO which formed on the alloy surface during annealing had to be removed by etching with pure hfacH in $scCO_2$. Figure S1b shows the surface after processing for 5 min in a 4.72 mM etching solution at 60°C and 145 bar. Figure S1c and d show the corresponding cross-sectional images of the layer before and after dealloying, respectively. It appears the dealloying reaction penetrated all of the way through the AgCu layer to the Ta diffusion barrier, but did not appreciably change the height of the film.

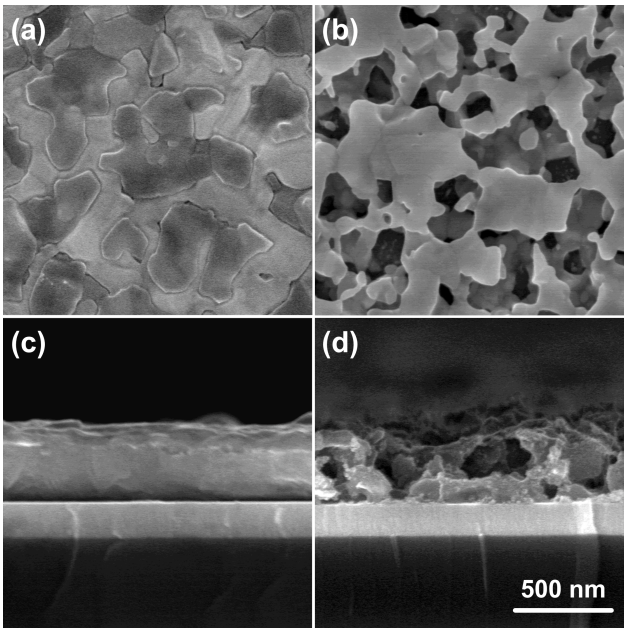

Figure S1: FESEM images of the AgCu films top-down (a) alloyed (b) dealloyed and cross-sectional (c) alloyed (d) dealloyed. Alloyed samples were heated at 450°C for 2.5 hours and dealloyed samples were processed for 5 min in a 4.72 mM etching solution at 60°C and 145 bar.

FESEM images of the early phases of dealloying

FESEM images from the early stages of AgCu dealloying revealed how the porous structure evolved. Figure S2a through d shows the AgCu surface after dealloying from 74.9% Cu to 70.6, 68.8, 63.4, and 60.1% Cu, respectively. The morphology progression from Figure S2a through d shows that as Cu was selectively removed in the Cu-rich phase, clusters of Ag formed and migrated toward the existing Ag-rich phase regions leaving pores.

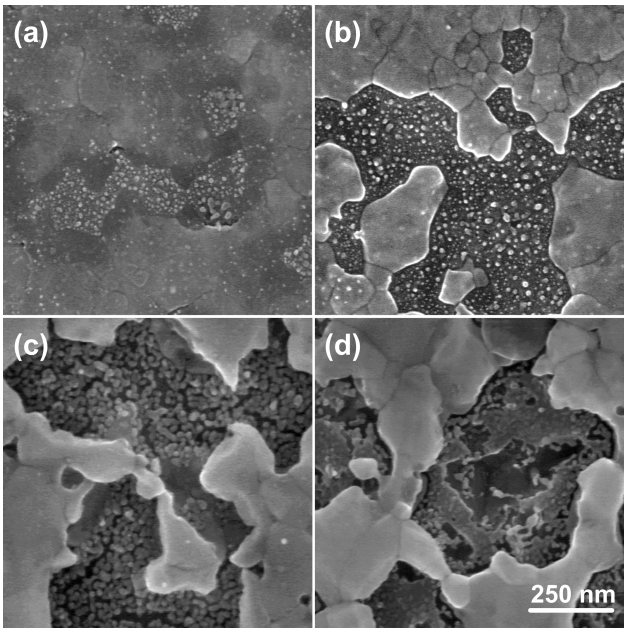

Figure S2: Top-down FESEM images of the AgCu films dealloyed to (a) 70.6 (b) 68.8 (c) 63.4 and (d) 60.1% Cu at 60°C and 145 bar.

Arrhenius plot of d for alloyed and dealloyed systems

Figure S3 shows an Arrhenius plot for the modeled size domain, d. Activation energies (E_A) were calculated between 450 - 700°C.

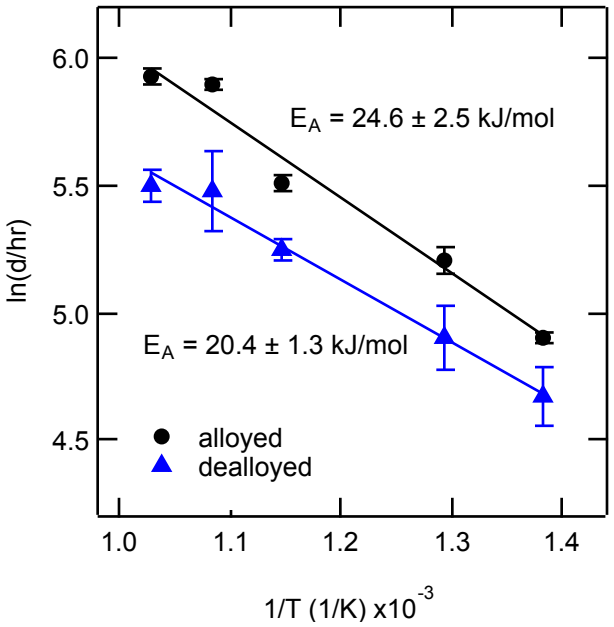

Figure S3: Arrhenius plot of size domain, d with E_A of 24.6 ± 2.5 for alloyed and 20.4 ± 1.3 kJ/mol for dealloyed images.

Description of FFT power spectrum model

Estimates of the feature size distribution in SEM images can be determined using inverse space image analysis. Images are typically analyzed using the power spectrum, $P(q)$, which is given by the square of the FFT magnitude, $F(q)$

$$P(q) = |F(q)|^2 = \int_a I(r)I(0)e^{[-j2\pi(q\cdot r)]}dr \qquad (1)$$

where I(r) is a 2-D discrete function with each point representing a gray scale intensity from a digital SEM image. The 2-D FFT power spectrum

directly corresponds to the intensity expected from a small angle scattering (SAS) profile, $S(q)$, where n represents the property responsible for scattering variations.

$$S(q) \propto \int_a n(r)n(0)e^{[-j2\pi(q\cdot r)]}dr \tag{2}$$

For image analysis of both the compositional and dealloyed FESEM micrographs, the 2-D FFT power spectra were rotationally averaged to reduce noise. The fundamental relationship between FFT power spectra and SAS scattering profiles indicates that the two techniques could be modeled similarly.

The model given as eq 1 in the primary manuscript is composed of two parts: a squared Lorentzian (SQL) function which was derived for scattering in random morphologies with distinct boundaries between phases and Ornstein-Zernike (OZ) scattering which can be derived from the small order parameter fluctuations of the Landrau free energy. OZ scattering is expected from variations in concentration, and in this case, represents gradients in contrast within the phase domains. This contrast arises from the SEM imaging process and can be attributed to variations of composition, height, and orientation in the samples. For example, when imaging highly topographic surfaces like the dealloyed samples, the secondary electron (SE) signal will be higher at edges causing these regions to appear brighter. In the alloyed images, compositional grading within the phases could have produced subtle variations in the atomic number contrast. Applying a threshold algorithm

to convert all contrast to either black or white can reduce the OZ scattering component, but was not used in our FFT analysis to avoid data loss. The OZ correlation length, ξ_2, represents the scale over which variations in contrast are connected within domain boundaries. Since size domain, d, grew at higher annealing temperatures, it is reasonable to expect a corresponding increase in the size scale of the contrast gradient. In all cases, ξ_2 was less than d, which supports assignment of OZ scattering to contrast variations within the light and dark regions of the images.